EARTH SURFACE PROCESSES AND LANDFORMS, VOL. 21, 853–868 (1996)

AN APPROACH TOWARDS DETERMINISTIC LANDSLIDE HAZARD ANALYSIS IN GIS. A CASE STUDY FROM MANIZALES (COLOMBIA)

C. J. VAN WESTEN AND M. T. J. TERLIEN

ITC, PO Box 6, 7500 AA Enschede, The Netherlands

Received 1 June 1995
Accepted 20 February 1995

ABSTRACT

A one-dimensional deterministic slope stability model (infinite slope model) was used to calculate average safety factors and failure probabilities for the city of Manizales, in central Colombia. An engineering geological data base has been created on the basis of a series of parameter maps (geology, geomorphology, Digital terrain models and slope classes), using logic reasoning in Geographic Information Systems (GIS). A two-dimensional hydrological model was applied to estimate groundwater levels in relation to rainfall events. A simple method for the calculation of horizontal seismic acceleration was used for different earthquake events. To calculate average safety factors a number of scenarios were developed, by combining the effects of groundwater and seismic acceleration with different return periods. A simple method for error propagation was used to calculate the variance of the safety factor, and the probability that it will be less than 1, for each pixel, within a time period of 20 years. The highest probability value of the various scenarios was selected for each pixel, and a final hazard map for translational landslides was constructed. The results presented here are a first approach towards a deterministic landslide hazard analysis using GIS. It has a number of drawbacks, which should be solved in future work.

KEY WORDS deterministic models; GIS; landslides; failure probability; rainfall; earthquakes; Colombia

INTRODUCTION

A large amount of research on landslide hazard zonation has been carried out over the last 30 years as the consequence of an urgent demand for slope instability hazard information for planning purposes. Overviews of the various slope instability hazard zonation techniques can be found in Hansen (1984), and Varnes (1984). Initially the investigations were oriented mainly towards problem solving at the scale of site investigation and development of deterministic models. A wide variety of deterministic slope stability methods is now available to the engineer. Reviews of these can be found in, for example, Graham (1984), and Anderson and Richards (1987). Deterministic, or physically based, models are based on physical laws of conservation of mass, energy or momentum. The parameters used in these models can be determined in the field or in the laboratory. Most deterministic models are site-specific and do not take into account the spatial distribution of the input parameters. Models which take into account the spatial distribution of input parameters are called 'distributed models'. Deterministic distributed models require maps which give the spatial distribution of the input data. The application of deterministic models for the zonation of landslide hazard in larger areas, however, has never seen a more extensive development, due to the regional variability of geotechnical variables such as cohesion, angle of internal friction, thickness of layers, or depth to groundwater. Furthermore, the calculation of safety factors over larger areas involves an extremely large number of calculations, which could not be executed without the use of Geographic Information Systems (GIS).

CCC 0197–9337/96/090853–16

Despite these problems, deterministic models are increasingly used in hazard analysis over larger areas. Currently, only the use of deterministic models will result in real hazard maps, according to Varnes's (1984) definition: 'Natural hazard means the probability of occurrence of a potentially damaging phenomenon within a specified period of time and within a given area'. Deterministic models, combined with the magnitude/frequency information of triggering events (rainfall, earthquakes), make it possible to derive a probability of failure, which can then be used in risk studies or in the design of engineering structures.

Deterministic slope stability models are only applicable in landslide hazard zonation when the geomorphological and geological conditions are fairly homogeneous over the entire study area and the landslide types are simple. In more heterogeneous areas they may lead to an undesirable generalization.

For the application of GIS in deterministic modelling, one-, two- or three-dimensional approaches can be followed. The most complex calculation procedure, using three-dimensional slope stability programs, requires the sampling of data at predefined grid-points, and export of these data to an external three-dimensional slope stability model. This is only applicable for very small areas, where a large amount of data is available, and is therefore not used in regional slope stability zonation.

Also the use of two-dimensional slope stability programs in a GIS environment is seldom used (Van Asch *et al.* 1993). This method requires the selection of a number of profiles from a digital terrain model (DTM) and other parameter maps. The resulting data are exported to external slope stability models. The main advantage of this approach is that externally existing models can be used without losing time in programming the model algorithms in a GIS. The disadvantages of model calculations outside GIS are data conversion, and the use of results of the model calculations in the construction of a landslide hazard map. The safety factors, calculated along the profiles, should be interpolated, or linked to geomorphological units, which may be very difficult.

The most suitable method for the use of deterministic models in a GIS environment is one-dimensional infinite slope modelling (Ward *et al.*, 1982; Brass *et al.*, 1989; Murphy and Vita-Finzi, 1991). It is the only model which calculates slope instability on a pixel basis, and is therefore very suitable to be used in a raster GIS.

The one-dimensional infinite slope model describes slope stability in the simplest form. It is only applicable for the calculation of shallow translational slides. Slope stability is calculated for the pixels on a map, using information combined from several input maps, such as slope angle, soil depth, soil strength, and depth to groundwater. Calculations for each individual pixel will result in safety factor values, which can be used to create a hazard map.

The basic formula for the infinite slope model is (after Graham, 1984):

$$F = \frac{c' + z(\gamma \cos^2 \beta - \rho a_h N \cos \beta \sin \beta - \gamma_w m \cos^2 \beta) \tan \varphi'}{z(\gamma \sin \beta \cos \beta + \rho a_h N \cos^2 \beta} \quad (1)$$

where F = safety factory, c' = effective cohesion (Pa), z = depth of failure surface below the terrain surface (m), which is equal to the thickness of ashes as we are assuming a failure surface at the base of the ashes, γ = unit weight of soil ($N\,m^{-3}$), β = terrain surface inclination (°), ρ = bulk density ($kg\,m^{-3}$), a_h = peak horizontal acceleration in rock ($m\,s^{-2}$), N = amplification of seismic acceleration in soil material (dimensionless), γ_w = unit weight of water ($N\,m^{-3}$), m = groundwater/soil thickness ration z_w/z (dimensionless), z_w = height of water table above failure surface (m), and φ' = effective angle of shearing resistance (°).

For calculation purposes Equation 1 was divided into two parts (Equation 2), later indicated as B_1 and B_2:

$$F = \frac{c'}{z(\gamma \sin \beta \cos \beta + \rho a_h N \cos^2 \beta)} + \frac{\tan \varphi'(\gamma \cos^2 \beta - \rho a_h N \cos \beta \sin \beta - \gamma_w m \cos^2 \beta)}{\gamma \sin B \cos \beta + \rho a_h N \cos^2 \beta} \quad (2)$$

THE STUDY AREA

In the framework of two international research projects, financed by the European Community, UNESCO and The Netherlands government, a methodology was developed for the use of GIS in landslide hazard

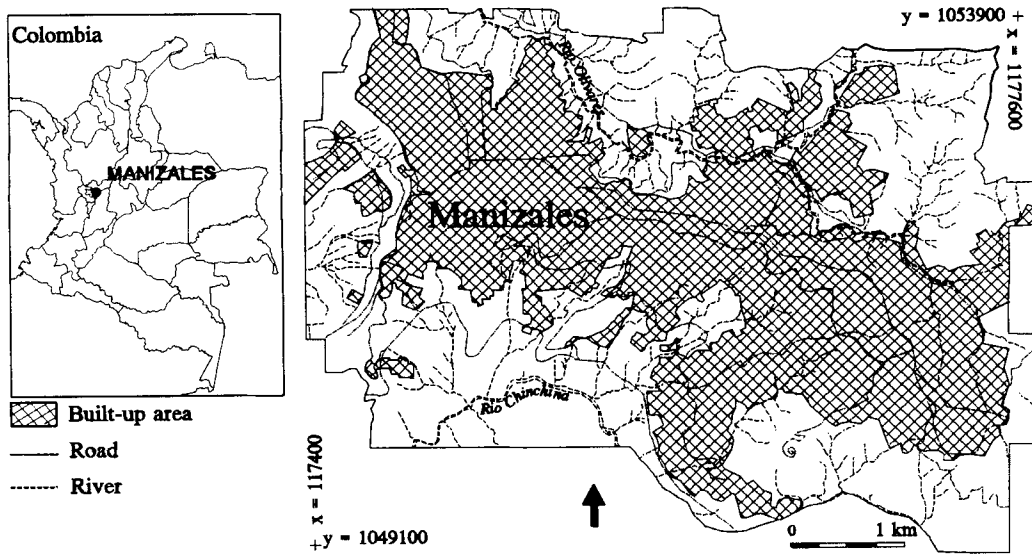

Figure 1. Location of the study area in Colombia

zonation (Van Westen *et al.*, 1993). The methods were tested in a study area in central Colombia, surrounding the city of Manizales (see Figure 1). Manizales (300 000 inhabitants) is located at an altitude of 2000 m on the western flank of the Cordillera Central, near the Nevado del Ruiz volcano. Owing to its unfavourable topographic location, large parts of the city are built on steep slopes, which are mostly modified by cuts and (hydraulic) fills to provide adequate terrain for housing. Manizales has suffered strongly from landslide problems. The landslides are a result of the geological and geomorphological setting of the area, the wet climate, and the fact that the area is located in a seismically active region. The geology of the area consists of metasedimentary schists of the Quebradagrande formation of Cretaceous age covered by fluvio-volcanic materials of Tertiary age (Manizales and Casabianca formations, consisting of debris flow material, pyroclastic flows, alluvial materials and intercalated ashes) with different degrees of weathering. Nearly the entire area is mantled by volcanic ashes of Quaternary age (Naranjo and Rios, 1989). The thickness of the ashes varies from 11 m on the flat hilltops to 1 m or less on very steep slopes. The ash deposits contain layers with textures ranging from very fine ($< 63\,\mu$m) to very coarse ($> 5000\,\mu$m) (Van Westen *et al.*, 1993). These changes in texture cause perched watertables in the ashes, which can trigger soilslips, soil avalanches, and translational slides. Most translational slides are caused by high groundwater levels in the volcanic ashes overlying impermeable residual soil developed on schists of the Quebradagrande formation.

THE INPUT DATA

To evaluate the stability of the entire city of Manizales on a general scale (1 : 10 000) the following steps were taken:

1. construction of an engineering geological data base;
2. groundwater modelling;
3. calculation of maximum horizontal seismic accelerations;
4. slope stability calculations using different scenarios for groundwater levels and seismic accelerations;
5. calculations of maximum failure probability within a given time period.

Engineering geological data base

Owing to the heterogeneous nature of the superficial materials in Manizales, its rugged topography and the small amount of drillhole information available, the engineering geological data base could not be obtained from interpolation of material depths, derived from drillholes and outcrops. Therefore, another method was developed based on the use of logic reasoning in GIS. With this method the spatial distribution of the various materials could be deduced from a very detailed geomorphological map, three landslide distribution maps from different periods, a geological map, and two DTMs from different dates with accompanying slope maps. Combining the different maps using conditional statements in GIS made it possible to produce the engineering geological data base. This data base describes the materials in three dimensions, showing both the spatial distribution of four basic material layers, and their thicknesses. As we are working with a two-dimensional GIS system (ILWIS) this was done by separating the spatial information from the thickness information (see Figure 2). In this way eight different maps were used which provide the soil profile for any pixel if they are read simultaneously using a pixel-information program. The maps show the spatial distribution of the four layers with the same material codes and can be linked with tables containing geotechnical properties derived from laboratory tests and field measurements. The procedure is explained in detail in Van Westen *et al.* (1993, 1994). One of the most important maps in the engineering geological data base is a map displaying the thickness of volcanic ashes. The thickness of these deposits is related to a large number of factors, such as the distance to the volcano, the slope angle and slope direction, the predepositional relief and the amount of erosion that has taken place. Initially a model was established for the calculation of maximum ash cover by means of multivariate statistical analysis, in which the ash thickness, derived from drillholes and outcrops, was used as the independent variable, and the other factors mentioned above, as dependent variables. From this analysis, only the slope angle turned out to be significant, so that finally a relation was made between ash thickness and slope angle only.

Groundwater simulations

In the case of deterministic landslide hazard zonation, distributed hydrological and slope stability programs are used to calculate the spatial distribution of piezometer levels and pore pressures. Also for hydrological models a choice can be made between one-, two- and three-dimensional models (Okimura and Kawatani, 1986; Terlien *et al.*, 1995; Terlien, 1996).

For the groundwater modelling a simple two-dimensional model was used (Van Asch *et al.*, 1992). This computer model calculates groundwater levels on a daily basis in layers with different hydrological properties.

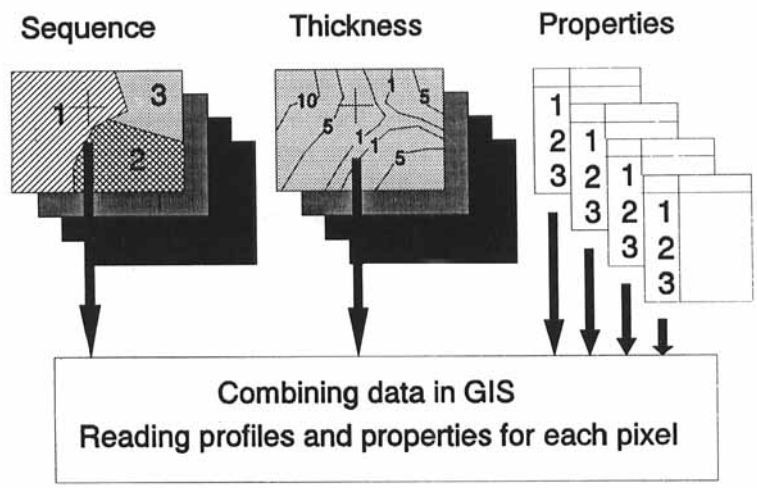

Figure 2. Simplified structure of the engineering geological data base for Manizales. Separate maps are made for the spatial distribution of materials (sequence), and for the thickness of materials. Profiles can be obtained by reading all maps simultaneously in GIS, and combining them with geotechnical properties from tables

As we were interested in the contact between volcanic ash materials and residual soils we applied a two-layer model to a large number of different profiles, with different values for slope angle, slope length, ash thickness, and saturated hydraulic conductivity. The saturated hydraulic conductivity of the first layer (ashes) was determined by field mesurements, using the inverse borehole method, and were within a range of 0·1 to 1 m per day. The differences in saturated hydraulic conductivity are closely linked with the grain-size distribution of the individual ash layers, which ranges from silt to sand. Since these layers alternate within a profile, with individual thicknesses of decimetres, and are not continuous throughout the area, it was decided to treat the entire ash cover as one layer. Whenever fill material derived from volcanic ashes was present, this was included in the first layer. The average saturated hydraulic conductivity of the second layer, composed of residual soil, was 0·005 m per day.

The maximum groundwater levels for each of these profiles were calculated for a 20 year period and used in the construction of magnitude–frequency curves Then the profiles were linked to the maps using the engineering geological data base and the topographic information, and groundwater maps were derived for different return periods (Van Westen *et al.*, 1993).

Seismic acceleration

In order to be able to calculate seismic acceleration, information should be available on the magnitude, frequency, and distance of seismic events, the material sequences, geotechnical data, groundwater levels, and topographic conditions. Unfortunately, no seismic data from accelerographs were available for the study area.

Many equations have been suggested to calculate peak ground acceleration for hard rock in relation to the magnitude and focal distance of seismic event (Hays, 1980). These equations are applicable only in those areas where they were developed. Donovan (1973) used worldwide data to derive a general equation:

$$a_h = 13{\cdot}2^{0{\cdot}58M}(R+25)^{-1{\cdot}52} \tag{3}$$

where a_h = peak horizontal acceleration for hard rock ($m\,s^{-2}$), M = magnitude (Richter scale), and R = hypocentre distance (km).

The value of 0·24 $m\,s^{-2}$, derived by this method for the 1979 earthquake (magnitude 6·3, distance to hypocentre 130 km) was approximately twice as low as the scarce values for acceleration at the surface, reported in Manizales (Geotecnia, 1980). This means that there is a strong amplification of the seismic waves due to topographic and geotechnical conditions.

A very simple estimation of the amplification of the seismic wave due to different materials can be obtained, derived from the work of Medvedev (1965):

$$N = 1{\cdot}67[\log_{10}(v_o\rho_o) - \log_{10}(v_1\rho_1)] + cf \tag{4}$$

where N = amplification of acceleration (dimensionless, v_o = seismic wave velocity of the material below the contact ($m\,s^{-1}$), ρ_o = bulk density of the material below the contact ($kg\,m^{-3}$), v_1 = seismic wave velocity of the material above the contact ($m\,s^{-1}$), ρ_1 = bulk density of the material above the contact ($kg\,m^{-3}$), and cf = correction factor for the depth of the phreatic water level. The acceleration values at the surface can be calculated by multiplying N (Equation 4) by the maximum acceleration in hard rock, derived from Equation 3.

In order to be able to calculate return periods for acceleration values, return periods are first selected for magnitudes of earthquakes. A record of 331 earthquakes occurring within the area between 4·5–6·0° north latitude and 74·5–76·5° west longitude was collected for the period 1922 to 1979 from the literature (James, 1986; Valencia, 1988; Page, 1986). On the basis of these data, the following relationship between magnitude and return period was calculated (Valencia, 1988):

$$M = 8{\cdot}2 - 2{\cdot}9\log(57/RY) \tag{5}$$

where M = magnitude on the Richter scale, and RY = return period in years.

To calculate maximum acceleration in hard rock for seismic events one must assume a distance to the hypocentre. A relatively short distance of 112 km was used (50 km to epicentre and 100 km depth of hypocentre), which is equal to the distance to the hypocentre of the 1962 earthquake. The resulting acceleration

Table I. Some values for peak acceleration at the rockhead (a_h), calculated for different earthquakes. Assumed distance to hypocentre is 112 km

Magnitude (Richter)	Return period (years)	Peak acceleration in rock, a_h ($m\,s^{-2}$)
7·5	32	0·578
6·9	20	0·408
6·5	15	0·324
6·0	10	0·242
5·5	7	0·214

values for several events are given in Table I. The data used to calculate amplification for a standard profile in the Manizales area are given in Table II (after Geotecnia, 1980).

Based on the values in Table II the amplification for different sequences of materials can be calculated from Equation 4. For example, a sequence of fill-ash–Manizales Formation–Quebradagrande Formation will result in an amplification value of $0{\cdot}48 + 1{\cdot}51 + 0{\cdot}23 = 2{\cdot}22$. A correction factor of 1 was used for groundwater occurring within 1 m below the surface and an amplification value of 0·5 for groundwater occurring between 1 and 4 m below the surface (James, 1986).

With data from Tables I and II and with the engineering geological data base, acceleration values can be calculated for each pixel for a given seismic event.

EVALUATING POSSIBLE FAILURE CONDITIONS

As mentioned in the Introduction, the use of even a very simple slope stability model is only feasible in relatively homogeneous terrain. Since the material thicknesses are the most crucial uncertainty in the analysis, an evaluation was made of the critical depth of translational landslides, by solving Equation 2 for the case $F = 1$. Based on this equation a number of different scenarios were evaluated.

In Figure 3 some of the values for the relationship between the depth of the sliding plane and the surface slope angle, derived from a set of translational landslides that were measured in the Manizales area, are plotted together with some critical depth lines for extreme conditions of c' and m. It is clear from this figure that landslides occur over a very wide range of soil thicknesses and surface slope angles. Slope angles are generally larger than 25°, and soil thicknesses range from 1 to 10 m. With the exception of one, all points are located between the maximum possible limits of cohesion and groundwater/soil depth relations. The conditions under which failure occurs are very different, and the use of one value for cohesion or groundwater/soil depth relation will lead to a simplification. The straight line displays the relationship between ash thickness and slope angle which was used to make an ash thickness map.

A calculation was made to estimate the number of pixels in the map that would have safety factors lower than 1 when the different conditions mentioned were applied (Table III). From this table it can be observed that groundwater/soil depth ratios of 0·5 and 1 lead to an extremely large percentage of pixels with a safety

Table II. Geotechnical properties of the main material types in the Manizales area, used to calculate seismic amplification (after Geotecnia, 1980)

Material	Seismic velocity, v ($m\,s^{-1}$	Bulk density, ρ ($kg\,m^{-3}$)
Fill	0·30	1300
Volcanic ash	0·38	1400
Manizales Formation	2·14	2000
Quebradagrande Formation	3·2	2600

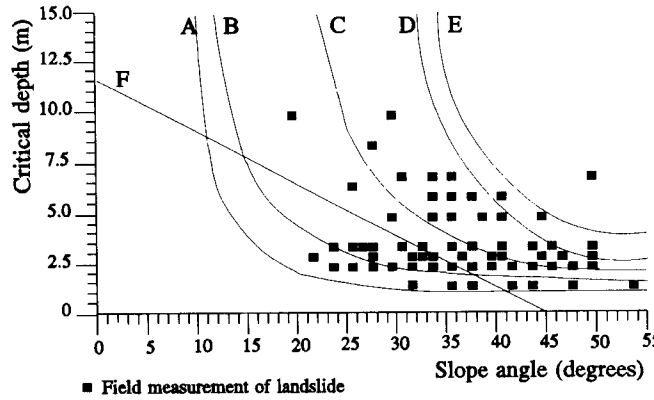

Figure 3. Values for the relationship between sliding plane depth and surface slope angle, measured for translational landslides in Manizales (■), plotted together with critical depth/slope angle relations calculated for some extreme values of cohesion (c') and groundwater/soil depth ratio ($m = z_w/s$). A, $c' = 5$ kPa, $m = 1$; B, $c' = 10$ kPa, $m = 1$; C, $c' = 10$ kPa, $m = 0{\cdot}5$; D, $c' = 10$ kPa, $m = 0$; E, $c' = 15$ kPa, $m = 0$; F, the relationship between ash thickness and slope angle which was used to make the ash thickness map

factor less than 1. This situation is, of course, very unlikely. Groundwater/soil depth ratios are not constant for different ash thicknesses. In the case of thin ash thicknesses this ratio may be as high as 1, and for thick ash it is seldom higher than 0·3. The influence of cohesion can also be evaluated from Table III. In the case of a cohesion of 5 kPa and an earthquake acceleration an unrealistically high percentage of the area is predicted to fail, even under dry conditions.

When the results of Table III are compared with Figure 3 it is clear that the map includes many other combinations of slope angle and ash or fill thickness than those predicted with the model (straight line in Figure 3). The reason for the deviation is the occurrence of fill material on top of the ash. Fill thickness was calculated as the difference in DTMs between 1949 and 1989. For those pixels with a fill thickness value that value was added to the thickness value coming from the straight line F in Figure 3. For those pixels where the terrain had been excavated, the excavation depth value was subtracted from the depth obtained from the straight line. The lower part of Table III displays the results of calculations performed on the fill materials. It appears that for 3700 pixels (1 per cent of the map area) the slopes will always fail, even in dry conditions and with high values for cohesion. This result must be due to errors in the DTMs and the slope maps.

Before the factor-of-safety maps were calculated it was considered important to remove the impossible combinations from the data set, caused by errors in the input data. The material maps obviously contain many combinations of soil thickness and slope angle, which are caused by errors in calculating fill thickness from DTMs. All points falling to the right of the curve showing critical depth for a cohesion of 15 kPa under dry conditions and without earthquake acceleration (line E in Figure 3) were displaced horizontally until they reached line E. This means that with any small increase of groundwater level or earthquake acceleration the terrain at these pixels will fail.

FACTOR-OF-SAFETY MAPS

Factor-of-safety maps were calculated, using Equation 2, for a number of scenarios, with different magnitudes of rainfall related groundwater levels, and seismic accelerations. Six scenarios were calculated:

1. dry condition, without earthquake;
2. groundwater with return period of 20 years, without earthquake;
3. completely saturated condition, without earthquake;
4. dry condition, with an earthquake of 6·9 Magnitude, with a return period of 20 years and occurring at a hypocentral distance of 112 km;

Table III. Percentage of pixels in the study area with ash and/or fill material failing under different conditions of c' (effective cohesion), a (seismic acceleration), and m (relation groundwater/soil depth). The lower section shows the error due to the presence of fill material

Effective cohesion c' (kPa)	Seismic acceleration at surface, a ($m\,s^{-2}$)	Groundwater/soil depth ratio m	Percentage of map with safety factor < 1
5	0	0	3
5	0	0·5	22
5	0	1	58
5	0·6	0	4
5	0·6	0·5	33
5	0·6	1	72
5	1·2	0	17
5	1·2	0·5	45
5	1·2	1	88
10	0	0	2
10	0	0·5	5
10	0	1	45
10	0·6	0	3
10	0·6	0·5	19
10	0·6	1	60
10	1·2	0	4
10	1·2	0·5	35
10	1·2	1	76
15	0	0	1
15	0	0·5	3
15	0	1	28
15	0·6	0	2
15	0·6	0·5	3
15	0·6	1	5
15	1·2	0	3
15	1·2	0·5	7
15	1·2	1	62
Calculation for pixels with fill only			
5	0	0	2
10	0	0	1
15	0	0	1

Table IV. Parameters used in the calculation of safety factors for six different scenarios. The parameters, used as maps, are given in **bold**. See Equation 1 for the definition of the parameters

	Scenarios					
Parameters in Equations 1 and 2	1	2	3	4	5	6
c' (Pa)	10000	10000	10000	10000	10000	10000
z (m)	**ASHT**	**ASHT**	**ASHT**	**ASHT**	**ASHT**	**ASHT**
γ (n m^{-3})	11000	14000	16000	11000	14000	14000
ρ (kg m^{-3})	1100	1400	1600	1100	1400	1400
a_h (m s^{-2})	0	0	0	0·408	0·408	0·408
N (-)	0	0	0	**N**	**N016**	**N20**
$\tan\varphi'$ (-)	0·58	0·58	0·58	0·58	0·58	0·58
γ_w (N m^{-3})	10000	10000	10000	10000	10000	10000
m (-)	0	**M20**	1	0	**M016**	**M20**

5. groundwater with return period of 0·16 years (occurring 2 months per year), and an earthquake with a return period of 20 years;
6. groundwater with return period of 20 years, and an earthquake with a return period of 20 years.

The parameters used in Equation 2 for the six scenarios are presented in Table IV. As can be seen from this table, some of the parameters are entered as values, and other are maps (shown in bold) related to different return periods.

The resulting factor-of-safety maps were classified into three classes, and the percentages of cover of the three classes were calculated (see Table V). The results show that the hypothetical scenario 3 – fully saturated conditions – will produce most landslides (31·9 per cent of the map has a safety factor smaller than 1).

The maps calculated on the basis of rainfall and earthquake are very similar, because a higher groundwater table as well as a high value of seismic acceleration have the same influence on the factor of safety. The combined effect of both a high groundwater level and a high value for earthquake acceleration will have a much stronger effect, but the probability that these two triggering events occur simultaneously is extremely low (less than 0·001). The map calculated for scenario 1 – dry conditions without an earthquake – gives a good indication of the error in the calculation. The 0·6 per cent with safety factors below 1, and part of the 3·4 per cent with values between 1·0 and 1·5, are due to the presence of fill material on top of ashes.

The classified factor-of-safety map calculated for scenario 2 is given in Figure 4. The strong relationship between the parameter maps (soil thickness, groundwater) and the slope angle is seen clearly in the map, as most of the areas with low safety factors occur on steep slopes. The slopes north and south of the central part of Manizales, where most of the squatter areas are located, have an especially high frequency of unstable areas. The slopes in the northeastern sector of the city, where future urbanization is planned, show a tendency to become unstable after extreme rainfall as well as due to earthquake events.

Table V. Percentage of study area with classified safety factors for six different scenarios

		Percentage for scenarios					
Class	Safety factory	1	2	3	4	5	6
1	0·1–1·0	0·6	11·4	31·9	1.3	15·9	18·8
2	1·0–1·5	3·4	15·1	20·0	18·6	18·9	18·5
3	>1·5	96·0	73·5	48·1	80·1	65·5	62·6

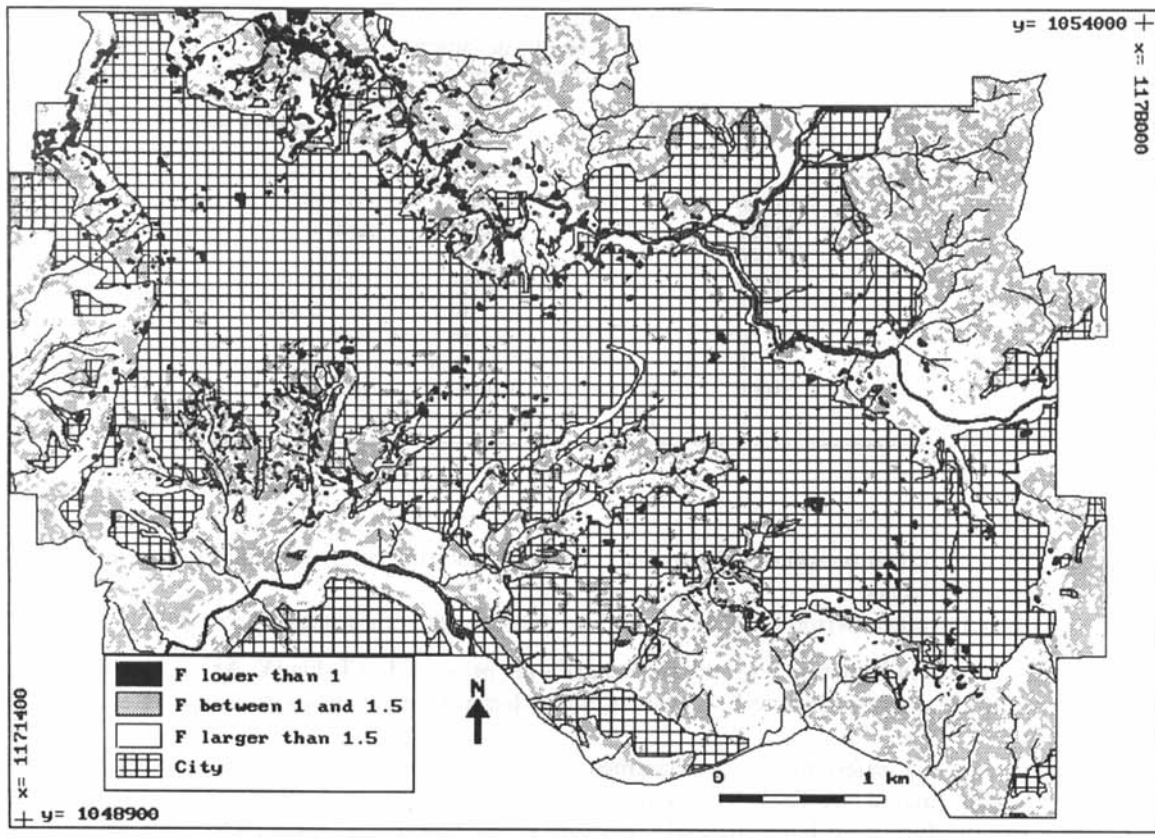

Figure 4. Classified factor-of-safety map for the study area calculated on the basis of groundwater levels related to a rainfall event with a return period of 20 years (scenario 2)

FAILURE PROBABILITY MAPS

In the previous section, a method to calculate safety factors was explained, which uses average values for the various input parameters. Most of these factors contain a large degree of uncertainty. For this reason, the use of safety factors calculated from average values is not recommended. It is better to present the maps as average safety factors plus or minus the standard deviation. Standard deviations and variances can be calculated in two ways;

- Stochastic methods are sometimes used for selection of input parameters (Mulder, 1991). Hammond *et al.* (1992) presented methods in which the standard deviation of the factor of safety is calculated from selected input variables following the Monte Carlo technique. This method requires a number of repeated calculations, normally between 200 and 100 000, which all have to be stored in separate maps. This makes the technique less suitable within a GIS.
- Another method for the calculation of the variance of safety factors is the use of error propagation techniques (Burrough, 1987; Heuvelink, 1993). This requires the construction of difficult equations, following rules for error propagation during arithmetical operations.

In this work a relatively simple formula for error propagation was used (Equation 6), based on Burrough (1987), which only takes into account the variance of the most important parameters (s, c' tan φ').

$$\mathrm{VAR}(F) = B_1^2\left(\frac{\mathrm{VAR}(c')}{z^2} + \frac{c'^2\mathrm{VAR}(z)}{z^4}\right) + B_2^2\mathrm{VAR}(\tan\varphi') \tag{6}$$

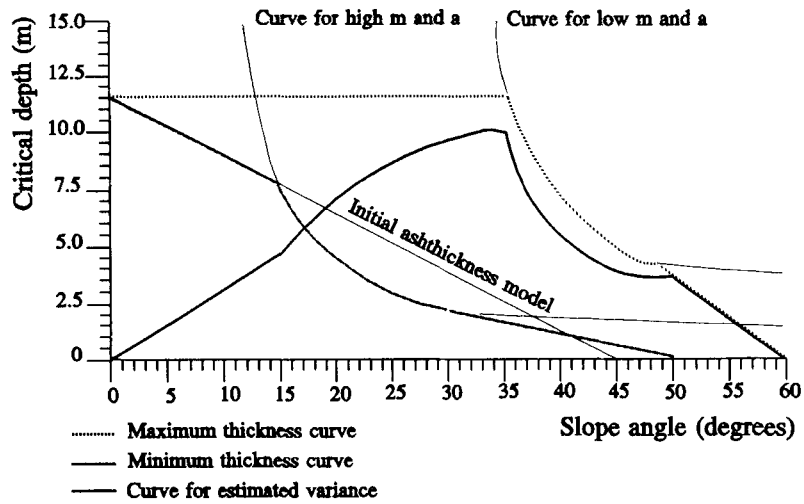

Figure 5. Method for deriving the variance of ash thickness. See text for explanation

where $\mathrm{VAR}(F)$ = variance of the safety factor, $\mathrm{VAR}(c')$ = variance of effective cohesion, $\mathrm{VAR}(\tan\varphi')$ = variance of the tangent of the effective friction angle, $\mathrm{VAR}(z)$ = variance of the ash thickness, B_1 and B_2 = the two separate terms of Equation 2.

The variances of the cohesion and the angle of internal friction for the ash deposits can be calculated from sampling point data. The standard deviations for ash deposits are in the order of 5 to 6 kPa for the cohesion, and 3 to 5° for the friction angle. The variance used here are 25 kPa for c' and 0·005 for $\tan(\varphi')$.

Determining the variance of ash thickness is much more difficult. From the field observations a very large variation of ash thickness for the same slope range was found. A simple calculation of standard deviations for each slope range would not yield satisfactory results. The approach that was chosen instead to determine the variance of ash thickness is based on the critical depth calculations, presented earlier in Figure 3. Based on a variable groundwater table, and different seismic acceleration values, it is possible to draw approximate upper and lower curves for critical depths (see Figure 5). In near-horizontal slopes the variance will be the lowest. It will increase slightly in slope ranges of 5 to 15°, depending on the amount of erosion. Once the critical depth curve is reached, the difference between the maximum and minimum critical depth will become very large, depending on differences in groundwater depth/soil thickness ratios (m). In the steeper slope ranges the variance becomes small again as the maximum and minimum curves approach each other. It is also assumed that due to erosion there will be no more ash cover at slope angles larger than 60°.

In calculating the variance of the safety factor, only the variances of cohesion, friction angle and soil thickness were taken into account. The variance of the groundwater depth/soil depth ration (m) and that of the seismic acceleration were too difficult to take into account. Based on these, partly hypothetical, variances of the input factors, the variance map for the safety factor was calculated, using Equation 6.

If it is assumed that the safety factors have a normal distribution, the deviation from the $F = 1$ value can be calculated. This deviation is expressed by a Z-value (Blalock, 1979):

$$Z = \frac{1 - \mathrm{AVG}(F)}{\sqrt{\mathrm{VAR}(F)}} = \frac{1 - \mathrm{AVG}(F)}{\mathrm{STD}(F)} \tag{7}$$

The Z-value can be considered as the distance between the average safety factor, $\mathrm{AVG}(F)$ which was calculated in the previous section, and $F = 1$, expressed in ordinates of Z-standard deviation. The total area under the normal curve is equal to 1. From a table of Z-values (Blalock, 1979) the area under the curve up to the

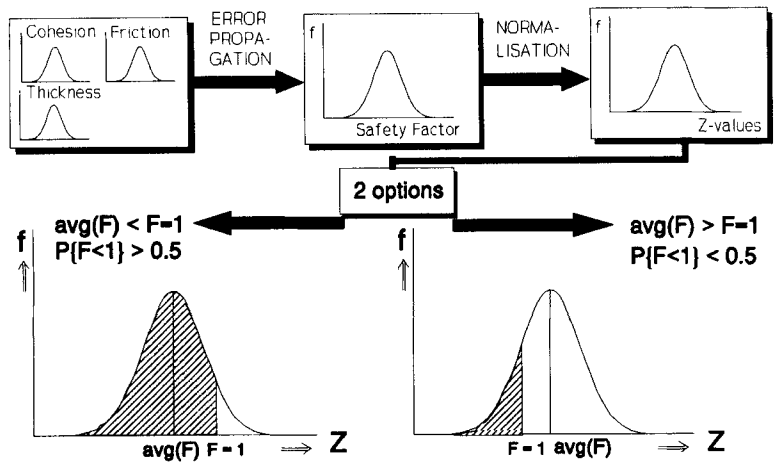

Figure 6. Schematic representation of the calculation of failure probability. See text for explanation

average safety factor can be obtained, which is equal to the probability that values lower than $F = 1$ can occur. A graphical presentation is given in Figure 6. The failure probability can be calculated for two different cases;

1. The left part of Figure 6 shows the failure probability for a positive Z-value. If $\mathrm{AVG}(F) < 1$ then $Z > 0$ (Equation 7) and the probability that $F < 1$ is formed by the total area indicated in the figure ($> 0{\cdot}5$).
2. The right part of Figure 6 shows the opposite case with a negative Z-value. If $\mathrm{AVG}(F) > 1$ then $Z < 0$ and the probability that $F < 1$ is formed by the total shaded area (< 0.5).

Probability maps were calculated for the six scenarios presented earlier. Figure 7 shows the distribution of the resulting probability classes for scenarios 2 and 5, with a differentiation of pixels with volcanic ashes and fill materials. It is clear from this figure that the pixels with fill materials, calculated from the differences in DTMs based on maps from 1949 and 1989, have the highest probability values.

The values for the failure probability calculated so far are only based upon the variance of the input parameters – cohesion, friction angle and soil thickness – given a certain magnitude for rainfall-related groundwater and/or seismic acceleration. To derive real probabilities, these values were multiplied by the probability that a given event, described in each of the scenarios, will occur within a given time period. In this case a design period of 20 years was used – the assumed design period for the low-budget housing projects in the Manizales area. Multiplication by the time probability will result in very low total probability values (which is the time probability multiplied by the probability based upon the variance of the input parameters) for scenarios 3, 5 and 6, due to their low time probability values. Scenario 3 – fully saturated conditions – is hypothetical, and will therefore result in final probability values of 0. For scenarios 5 and 6 the final values will be very low, as the probability that both a rainfall event and an earthquake occur on the same day will be low.

For the calculation of the overall hazard map for Manizales, all possible scenarios with respect to the magnitudes of the triggering factors should be calculated, and the results presented as probability values within a 20 year design period. Fortunately, a number of scenarios with combined rainfall and earthquake effects can be neglected, as their time probability will be so low that it will not be significant. Therefore, a selection was made of 15 scenarios, with the effect of one single triggering factor only. Out of the 15 maps produced for each of these scenarios, the highest probability value was selected for each pixel. The resulting map is given in Figure 8. This map shows values up to 1 in the steep squatter areas north and south of the city centre. In those areas, it will be very likely that a translational slide may occur within a 20 year period.

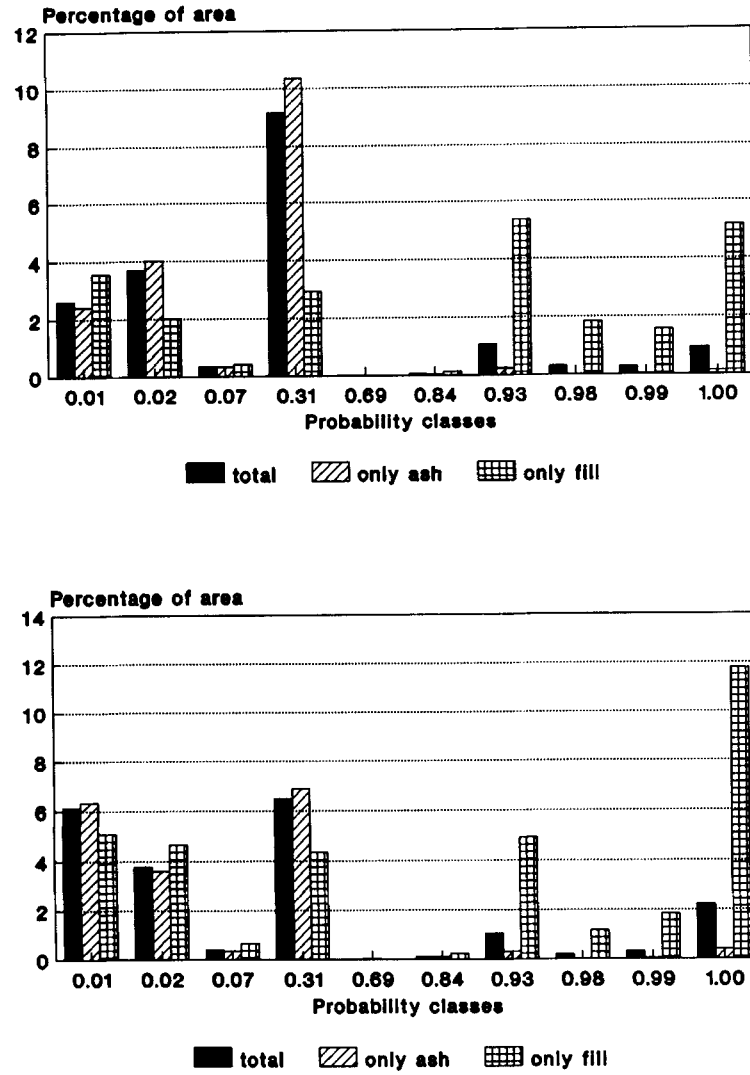

Figure 7. Classes for failure probability calculated using an infinite-slope model, calculated for two scenarios. Only probability values larger than 0 are displayed. Top: scenario 2. Bottom: scenario 5

DISCUSSION AND CONCLUSIONS

The final hazard map was checked with the occurrences of landslides. From the landslide distribution maps from the 1960s and 1980s, only the scarps of surficial translational landslides, that had occurred between 1960 and 1990, were selected. The resulting map was overlain with the hazard map. The result shows that 2·4 per cent of the landslide scarps were in places with pixels having a probability larger than 0·1. This is not a very good indication, as it is not required that all pixels within a potential landslide should have high probability values. If the individual landslides are evaluated, 62 per cent of the 438 landslides had pixels with a probability larger than 0·1. This means that 38 per cent of the shallow translational landslides were not predicted. This may be caused by the fact that they did not occur in volcanic ashes, or that the landslide occurred within the ash deposits themselves, and not on the contact between ashes and residual soils, for which the hazard map is made.

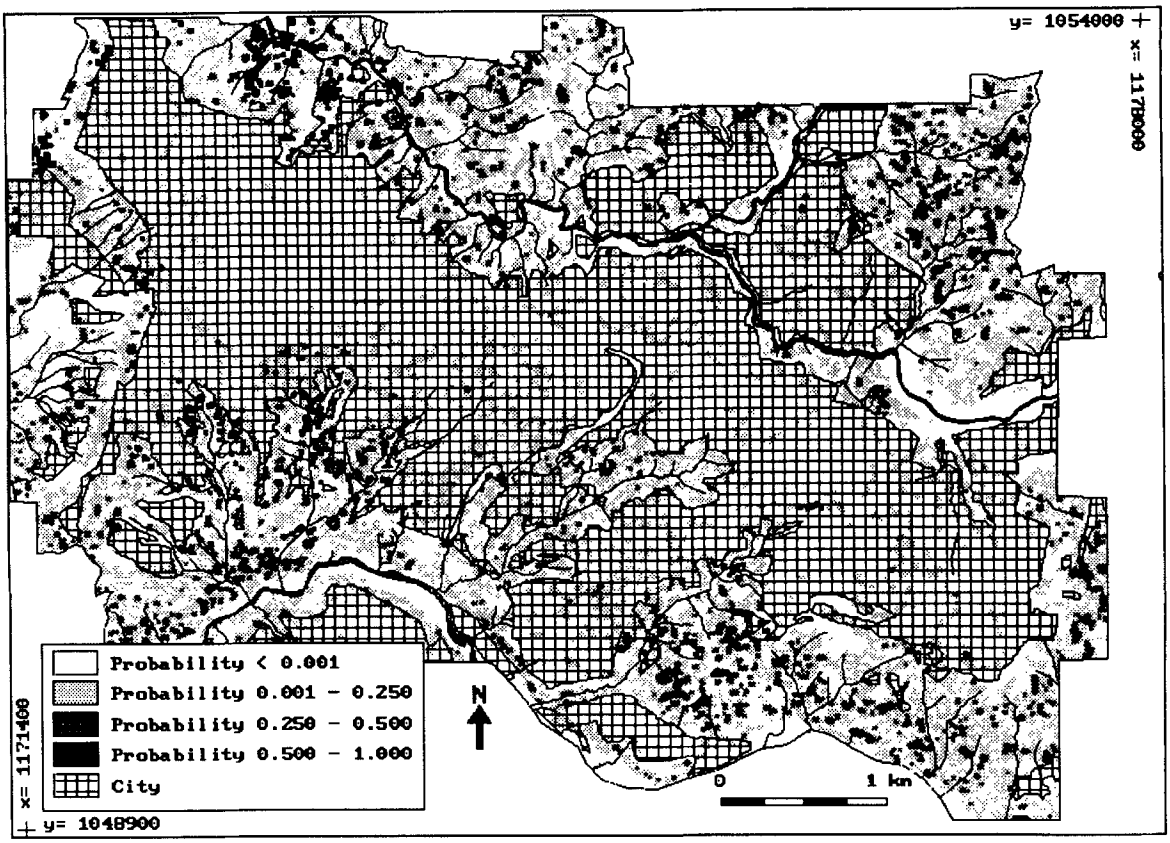

Figure 8. Final probability map for translational slides within a 20 year design period

To test the accuracy of the actual probability values, the hazard map was overlain with the total landslide distribution map of the 1980s. Of all pixels with a probability between 0·1 and 0·5, 20 per cent were actually covered by landslides, and for the pixels with a probability larger than 0·5, 26 per cent. For this last group the expected value should be somewhere around 75 per cent. This difference is caused mainly by the presence of fill materials on top of ashes, which have probability values that are too high (see Figure 7). This leads to the conclusion that the resulting safety factors and probability values should not be used as absolute values. They are only indicative and can be used to test different scenarios of slip surfaces, groundwater depths, and seismic accelerations. They can also be used to analyse the sensitivity of the various input parameters.

The method presented here has a series of drawbacks, which should be taken into account.

- The ash thickness map based on the model line (line F in Figure 3) is a rather conservative estimation. Most of the pixels are stable under groundwater/soil thickness ratios smaller than 0·5, even when earthquake acceleration is taken into account. In reality, soil thickness may be much larger than calculated in the model.
- When fill thicknesses are used the situation is reversed. More than a realistic number of pixels with fill material will fail even under normal conditions (Figure 7). This is caused by errors in the DTMs and by the assumptions that the fill material is deposited on top of ashes. The soil thickness map, which was used in this study, is only a rough approximation of the real situation. More research should be carried out to obtain a better model for ash thickness, and the errors in the DTMs should be reduced.
- The landslide hazard map was only calculated for the occurrence of translational slides on the contact of volcanic ashes and/or fills, and residual soils. For the inclusion of other landslide types and failure mechanisms, other methods should be used.

- The groundwater map is made using a simple two-dimensional hydrological model. Accumulation of groundwater related to slope length or concavity was not taken into account. More research is required to incorporate three-dimensional hydrological models in the analysis (Terlien *et al.*, 1995; Terlien, 1996).
- The soil variables (cohesion, friction angle, density and saturated conductivity) are assumed to be uniform for the same material, throughout the area. In future studies, the spatial variability of the soil strength values should also be taken into account.
- For determining seismic acceleration values empirical relations, developed in other areas, were used. Topographic amplification was not taken into account. Local information from accelerographs is required to update these values.
- For the probability calculation only the variance of ash thickness, cohesion and friction angle were taken into account.
- No effects of the city itself, such as loading by houses, impervious terrain surfaces, leaking water pipes, or stabilization measures, were included in the calculations.
- The model which was used only outlines the initiation points of the landslides. Many landslides in the area occur as soil avalanches, which destroy even more houses in the transportation zone. Neighbourhood analysis should be used to model these areas, based on the initiation points provided by the map of Figure 8.

The list of drawbacks makes clear that only general conclusions can be drawn from the resulting maps. The probability map for translational landslides should be used, in combination with landslide distribution maps and hazard maps for other landslide types, to make a general zonation map. The improvement of the resulting hazard map by collecting more data may be very difficult, as many variables are very heterogeneous within an urban area like Manizales. The method may be more applicable over more homogeneous areas at a large scale (over 1 : 10 000).

ACKNOWLEDGEMENTS

The authors wish to thank the following persons for their valuable contribution: Niek Rengers, Rob Soeters, Jan Rupke, Theo van Asch, Jean Pierre Asté, Ofelia Tafur, Carlos Enrique Escobar, Henk Kruse, Juan B. Alzate, Dinand Alkema, Marnix Mosselman, Jose Luis Naranjo, Monica Dunoyer, Pradeep Mool, Achyuta Koirala and Eric Mählman.

This work was financed by the EC, UNESCO, The Netherlands Ministry for Education and Science and ITC.

REFERENCES

Anderson, M. G. and Richards, K. S. (Eds) 1987. *Slope Stability. Geotechnical Engineering and Geomorphology*, Wiley & Sons, New York, 648 pp.

Blalock, H. M. 1979. *Social Statistics*, McGraw Hill, New York, 625 pp.

Brass. A., Wadge, G. and Reading, A. J. 1989. 'Designing a Geographical Information System for the prediction of landsliding potential in the West Indies', *Proc. Economic Geology and Geotechnics of Active Tectonic Regions*, University College, London, 3–7 April 1989, 13 pp.

Burrough, P. A. 1987. *Principles of Geographical Information Systems for Land Resources Assessment*, Clarendon Press, Oxford, 194 pp.

Donovan, N. C. 1973. 'A statistical evaluation of strong motion data including the February 9, 1971 San Fernando earthquake', *Proc. Fifth World Conference on Earthquake Engineering*, Rome, Italy, Vol. 2, paper 155, 10 pp.

Geotecnia LTDA 1980. *Investigacion geotecnica postsismica del sector de la avenida Santander entre la Calles 47 y 48*, unpublished report for the Corporacion Regional Autonoma de Manizales, Salamina y Aranzazu (CRAMSA), Manizales, Colombia, 30 pp.

Graham, J. 1984. 'Methods of stability analysis', in Brunsden, D. and Prior, D. B. (Eds), *Slope Instability*, Wiley & Sons, New York, 171–215.

Hammond, C. J., Prellwitz, R. W. and Miller, S. M. 1992. 'Landslide hazard assessment using Monte Carlo simulation' ,*Proc. Sixth International Symposium on Landslides*, Christchurch, New Zealand, Vol. 2, 959–964.

Hansen, A. 1984. 'Landslide hazard analysis', in Brunsden, D. and Prior, D. B. (Eds), *Slope Instability*, Wiley & Sons, New York, 523–602.

Hays, W. N. 1980. *Procedures for Estimating Earthquake Ground Motions*, US Geological Survey Professional Paper 1114, 77 pp.

Heuvelink, G. B. M. 1993. *Error Propagation in Quantitative Spatial Modelling*, Nederlandse Geografische Studies 163, University of Utrecht, 151 pp.

James, M. E. 1986. *Estudio sismotectonico en el area del viejo Caldas*, internal report no. 2008, Instituto de Geologia y Minas (INGEOMINAS), Medellin, Colombia, 113 pp.

Medvedev, A. 1965. *Engineering Seismology*, National Technical Information Service (NTIS), TT 65-50011, 260 pp.

Mulder, H. F. H. M. 1991. *Assessment of Landslide Hazard*, Nederlandse Geografische Studies, 124, University of Utrecht 150 pp.

Murphy, W. and Vita-Finzi, C. 1991. 'Landslides and seismicity: an application of remote sensing', *Proc. Eighth Thematic Conference on Geological Remote Sensing (ERIM)*, Denver, Colorado, USA, Vol. 2, 771–784.

Naranjo, J. L. and Rios, P. A. 1989. 'Geologia de Manizales y sus alrededores y su influencia en los riesgos geologicos', *Revista Universidad de Caldas*, **10**(1–3).

Okimura, T. and Kawatani, T. 1986. 'Mapping of the potential surface-failure sites on granite mountain slopes', in Cardiner, J. (Ed.), *International Geomorphology*, Part 1, Wiley, Chichester, 121–138.

Page, W. (Ed.) 1986. *Geologia sismica y sismicidad del noroeste de Colombia*, Interconexion Electrica SA, Medellin, 277 pp.

Terlien, M. T. J. 1996. *Modelling Spatial and Temporal Variations in Rainfall-Triggered Landslides*. ITC Publication Number 32, ITC, Enschede, The Netherlands, 254 pp.

Terlien, M. T. J., Van Asch, Th. W. J. and Van Westen, C. J. (1995). 'Deterministic modelling in GIS-based landslide hazard assessment', in: Carrara, A. and Guzzetti, F. (Eds) *Advances in Natural and Technological Hazard Research*, Kluwer, 57–77.

Valencia, C. E. 1988. *Geotectonica regional del antiguo Caldas con enfasis en la aplicacion a la ingenieria sismica*, unpublished MSc thesis, Universidad de los Andes, Bogotá, Colombia, 54 pp.

Van Asch, T. W. J., Van Westen, C. J., Blijenberg, H. and Terlien, M. 1992. 'Quantitative landslide hazard analyses in volcanic ashes of the Chinchina area, Colombia', *Proc. 1er Simposio Int. sobre Sensores Remotes y Sistemas de Informacion Geografica para el estudio de Riesgos Naturales*, Bogotá, Colombia, 10–12 March 1992, 433–443.

Van Asch, Th. W. J., Kuipers, B. and Van der Zanden, D. J. 1993. 'An information system for large scale quantitative hazard analysis of landslides', *Zeitschrift für Geomororph. NF*, Suppl. -Bd **87**, 133–140.

Van Westen, C. J., Van Duren, I., Kruse, H. M. G., and Terlien, M. T. J., 1993. *GISSIZ: training package for Geographic Information Systems in Slope Instability Zonation*, ITC Publication Number 15, ITC, Enschede, The Netherlands. Vol. 1 Theory, 245 pp, Vol. 2 Exercises, 359 pp, 10 diskettes.

Van Westen, C. J., Rengers, N., Soeters, R. and Terlien, M. T. J. (1994).'An engineering geological GIS data base for mountainous terrain', *Proc. 7th Cong. IAEG*, Balkema, Rotterdam, 4467–4475.

Varnes, D. J. 1984. *Landslide Hazard Zonation: a review of principles and practice*, UNESCO, Natural Hazards, No 3, 61 pp.

Ward, T. J., Ruh-Ming, L. and Simons, D. B. 1982. 'Mapping landslide hazards in forest watershed', *Jopurnal of Geotechnical Engineering Division, Proceedings of the American Society of Civil Engineers*, **108**(GT2), 319–324.